The Astrophysical Journal, 950:23 (13pp), 2023 June 10 https://doi.org/10.3847/1538-4357/acca1b

Properties of Forbush Decreases with AMS-02 Daily Proton Flux Data

Siqi Wang, Veronica Bindi, Cristina Consolandi, Claudio Corti, Christopher Light, Nikolay Nikonov, and Andrew Kuhlman
Physics and Astronomy Department, University of Hawai'i at Mānoa, 2505 Correa Road, Honolulu, HI 96822, USA; siqiwang@hawaii.edu
Received 2022 October 17; revised 2023 March 3; accepted 2023 April 2; published 2023 June 7

Abstract

A Forbush decrease (FD) is a sudden reduction of Galactic Cosmic Rays (GCRs) that is usually caused by intense solar wind transients, such as Interplanetary Coronal Mass Ejections (ICMEs) and Corotating Interaction Regions (CIRs). Using daily proton fluxes measured by AMS-02 between 2011 May and 2019 October, we identified 142 FD events with an automatic systematic analysis method. The properties of 47 FDs caused by ICMEs and of 54 FDs caused by CIRs were analyzed. We found that the rigidity dependence of the GCR flux decrease is generally better described by an exponential function for both ICME and CIR FDs. We also found that the FD Amplitude of ICME FDs has a moderate correlation with the minimum Dst index and a number of solar wind parameters, such as maximum temperature, pressure, and magnetic field. For CIR FD events, neither FD Amplitude nor Maximum Affected Rigidity had a significant correlation with solar wind parameters.

Unified Astronomy Thesaurus concepts: Forbush effect (546); Galactic cosmic rays (567); Solar coronal mass ejections (310); Corotating streams (314); Solar activity (1475)

1. Introduction

The intensity of the Galactic Cosmic Ray (GCR) spectrum inside the heliosphere is modulated by solar activity on multiple timescales. Forbush decreases (FDs) (Forbush 1937) are sudden reductions of GCRs, which happen within hours or days and are followed by a recovery period that lasts from one day to several weeks. Although FDs can be associated with all sorts of solar wind perturbations, the primary causes of FDs are considered to be Interplanetary Coronal Mass Ejections (ICMEs) and Corotating Interaction Regions (CIRs).

ICMEs are large-scale magnetized plasma structures that are ejected from the solar surface into interplanetary space. They usually contain a magnetic cloud with a shock in the front followed by a turbulent sheath. ICMEs act as barriers to GCRs propagating through them. As a consequence, GCR intensities are suddenly suppressed, sometimes taking weeks to recover to previous levels. In solar wind data, ICME shocks can be identified by a rapidly increasing solar wind speed and magnetic field intensity, whereas magnetic clouds can be identified by a depressed temperature and a rotating magnetic field (Cane 2000).

CIRs, or stream interaction regions, are caused by fast corotating solar wind streams originating from coronal holes (Richardson 2018). The high speed streams create a forward shock when they meet the slow ambient solar wind and form interaction regions, which are called corotating interaction regions. CIRs can cause FDs with a gradual decrease and are usually followed by a symmetric recovery. When the coronal holes last more than one solar rotation, the CIR becomes recurrent and can cause recurrent FDs.

FDs are traditionally studied with ground-based Neutron Monitors (NMs) (see, e.g., Usoskin et al. 2008 and references therein) and balloon experiments (Clem et al. 1993). It has generally been postulated that there is a power-law relation between the decrease amplitude and the rigidity R of the GCRs: amplitude $\propto R^{-\gamma}$. Estimates for γ, or the amplitude spectral index, ranges from about 0.4 to 1.2 according to Cane (2000), or mostly within 0.3 to 0.7 according to Belov et al. (2021), depending on the period of observation and instruments used. Ahluwalia & Fikani (2007) studied the dependence of FD amplitude on the median rigidity of response (Rm) of NMs, below which lies 50% of the detector counting rate, and found a perfect correlation (>0.99 computed in log-log space) between FD amplitude and the Rm for three significant FD events, which indicates that there is a power-law relation between the amplitude and the Rm: amplitude $\propto \mathrm{Rm}^{-\gamma}$. Some studies of the time evolution of γ during FDs have shown that γ decreases during the decrease phases of FDs (i.e., the spectrum hardens) and that γ increases during the recovery phases of FDs (i.e., the spectrum softens) (Alania & Wawrzynczak 2008, 2012). However, other studies have shown that the dynamics of γ at different phases of FDs varies highly from one event to another and that there are no clear regularities (see, e.g., Klyueva et al. 2017 and references therein; Belov et al. 2021). In recent years, a number of space-born detectors have obtained direct measurements of cosmic-ray spectra in space, which enabled the study of the FD rigidity dependence directly with primary particle fluxes. Munini et al. (2018) studied the December 2006 FD event with proton, helium, and electron data measured by PAMELA . Using PAMELA proton data from 0.4 to 20 GV, they concluded that an exponential fit (amplitude $\propto e^{-\alpha R}$) is more suitable to describe the rigidity dependence of the amplitude than a power-law fit. They also show that the helium and the proton amplitude are in agreement within the errors for each rigidity interval from 1 to 10 GV, which suggests that the exponential description of the rigidity dependence might be extrapolated to helium to some degree. Alemanno et al. (2021) studied the 2017 September FD event with the CRE (cosmic-ray electron and positron) fluxes observed by the Dark Matter Particle Explorer (DAMPE) and also found that the amplitude can be well described by an exponential function in terms of

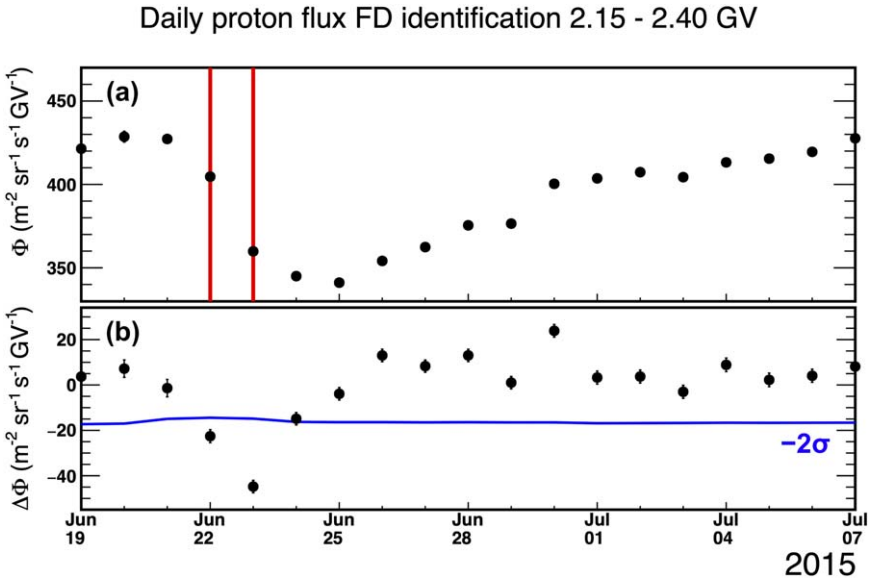

Figure 1. An example of FD identification in the rigidity bin from 2.15 to 2.40 GV, between 2015 June 19 and 2015 July 7. (a) AMS-02 daily proton fluxes. Error bars are smaller than the marker size. Red lines, on 2015 June 22 and 2015 June 23, mark the days recognized as significant decreases. (b) The flux difference between each day and the previous day. The blue line indicates the -2σ threshold for significant flux decrease. See the text for the error definition.

energies. Thus, the rigidity dependence of FDs remains a very complicated problem and needs to be further studied. In this paper, for the first time, we study the rigidity dependence of a large number of FD events, of different origins, using the precise daily proton data, in the rigidity range from 1 to 100 GV, that were measured by the Alpha Magnetic Spectrometer (AMS-02) on the International Space Station (Aguilar et al. 2021) from 2011 May 20 to 2019 October 29.

There is often a discrepancy between lists of events measured by various instruments due to their different observational positions, times when solar wind transients cross them, measured particle species, and energy ranges. Therefore, in this paper, we derive a list of FDs using only AMS-02 daily proton fluxes.

In Section 2, we describe the method used to identify FDs in the AMS-02 daily proton flux and how we categorize them into ICME FDs and CIR FDs. In Section 3, we study the rigidity dependence of the identified FD events and explain how we define the FD Amplitude and Maximum Affected Rigidity (MAR). In Section 4, we present the correlation between FD properties and solar wind parameters. In Section 5, we give a summary of this paper.

2. FD Identification

To identify FDs in AMS-02 proton data, we developed an automated method to find significant decreases in the daily flux. The rigidity range that we used to recognize the onset of FDs is from 1 to 10 GV, in 22 rigidity bins, because this is the most affected rigidity range during FDs. A significant daily decrease is computed similarly to Light et al. (2020): we calculate the flux difference, $\Delta\Phi_d$, between each day and its previous day for all 180 days before the day of interest: $\{\Delta\Phi_d \,|\, \Delta\Phi_d = \Phi_d - \Phi_{d-1},\ d = 1, 2,...,180\}$, where Φ_d is flux value at day d. The threshold on the day of interest is calculated as twice the standard deviation (σ) of the 180 flux differences.[1] If the daily flux at any rigidity below 10 GV decreases by more than 2σ, i.e., the flux difference $\Delta\Phi$ is below -2σ, then this day is recognized as a "significant decrease". Here the error is also taken into account: $\Delta\Phi_d + \delta\Delta\Phi_d < -2\sigma$, where $\delta\Delta\Phi_d$ is the error of the flux difference. The flux errors are the quadratic sum of statistical and systematic time-dependent errors (the systematic time-independent errors were excluded because they only affect the overall flux normalization and not the relative variation). An example of this method is shown in Figure 1. Figure 1(a) shows the proton flux from 2.15 to 2.40 GV from 2015 June 19 to 2015 July 7. Significant decreases are marked on June 22 and June 23 by the red lines. Figure 1(b) shows the corresponding flux difference. The blue line marks the -2σ threshold.

The σ threshold denotes the background level of the flux fluctuations around the day of interest due to the variability of interplanetary conditions. The σ value is higher during solar maximum than during solar minimum because the level of solar activity is higher. During such periods, a higher σ is needed to filter smaller fluctuations that are not associated with solar wind transients.

With this method, 180 preliminary significant decreases were selected, from 2011 May 20 to 2019 October 29. Note that, as shown in Figure 1, significant decreases can occur on successive days if the flux keeps decreasing more than the threshold for multiple days in a row. Most of the time, these continuous significant decreases are associated with the same solar wind transient, so they are all considered to be part of the same single FD event. Meanwhile, we identified the causes of the FDs by referring to ICME catalogs from Richardson & Cane (2010) and Nieves-Chinchilla et al. (2018), and to CIR catalogs from Grandin et al. (2019) and Maris Muntean et al.[2] For each event, we also checked the solar wind parameters from NASA OMNIWeb.[3] Using this procedure, we found 142 FD events in total, of which 55 were associated with ICME FD events, 58 were associated with CIR

[1] If the day of interest is within the first 180 days after 2011 May 20, then σ is calculated using the 180 days after 2011 May 20 (data gaps within the 180 days were excluded).

[2] http://www.geodin.ro/varsiti/

[3] https://omniweb.gsfc.nasa.gov/

FD events, 6 were caused by a combination of ICMEs and CIRs, and 23 were of unknown origin (i.e., not categorized). All of the FD events and their associated solar activities are listed in the Appendix.

3. FD Characteristics

The characteristics of ICME and CIR FDs were studied using the daily AMS-02 proton flux from 1 to 100 GV, in 30 rigidity bins. For each of these events, we defined the following characteristics:

1. *Decrease date:* the first day of significant decrease recognized by the method described in Section 2.
2. *Disturbance date:* the date of disturbance of the corresponding ICME or CIR according to Richardson & Cane (2010), Grandin et al. (2019), or Maris Muntean et al. (see Footnote 2). For ICMEs, this is the time of the associated geomagnetic storm sudden commencement, which is typically related to the arrival of a shock at Earth. For CIRs, it is when the magnetic field intensity and the solar wind speed start to rapidly increase. The date of disturbance is usually the same day as the decrease date or one day before.
3. *Minimum flux day:* the day when the majority of rigidity bins below 10 GV reach their minimum flux.
4. *Rigidity dependence:* the rigidity spectrum during the FD normalized by the rigidity spectrum on the reference date.
5. *Reference date:* to study the effect of a specific disturbance, the reference date is chosen as the day before the disturbance date.

As an example, Figure 2 shows the time profiles of an ICME FD event and a CIR FD event. The reference date, disturbance time, and minimum flux day are marked with arrows.

Even though the duration of a FD can last from one day to several weeks, in this work, we decided to study the rigidity dependence on the minimum flux day only, which is the most representative of the event decrease and is less contaminated by the recovery phase. The onset and the recovery phases are not studied because: (1) although the two-step decrease of ICME FDs is important to distinguish the effects of ICME sub-structures (see , e.g., Janvier et al. 2021 and references therein), this process usually happens within one day and cannot not be seen with a daily time resolution; (2) we found that the majority of the FD recovery phases are usually affected by other solar wind transients, which makes it very difficult to disentangle cause and effect. However, these studies might be performed on a restricted set of isolated ICME and CIR events, which will be a subject of a future study. Nevertheless, we present an example of the time evolution of the rigidity spectrum in Figure 3 Section 3.1.

3.1. FD Rigidity Dependence

It is traditionally postulated that the FD amplitude spectrum can be modeled as $\delta\Phi/\Phi \propto R^{-\gamma}$ (Cane 2000; Alania & Wawrzynczak 2008, 2012; Belov et al. 2021). Similarly, we fit the normalized rigidity spectrum during the FD with a power-law function:

$$\Phi_{\rm norm} = C' - b \cdot R^{-\gamma} \quad (1)$$

where C' is the asymptotic value of the normalized rigidity spectrum at very high rigidities (which is expected to be around 1 given that the modulation effects at 100 GV should be negligible), b is the decrease amplitude at 1 GV, and γ controls the rise in the normalized rigidity spectrum. This function is not completely physical because it can become negative below 1 GV. However, it is well behaved in the analyzed rigidity range (i.e., above 1 GV). Note that Equation (1) is related to past studies by $\delta\Phi/\Phi = 1 - \Phi_{\rm norm}$ when $C' = 1$. Thus, the values of γ found in this work should be directly comparable with the values of γ found in the literature.

Figure 3 shows the time evolution of the rigidity dependence during an FD event that occurred on March 8, 2012, as an example. This event is the largest FD analyzed in this paper in terms of amplitude. The fluxes are normalized by the flux on March 7, which is one day before the onset of the FD. The near-Earth heliospheric environment was relatively quiet on March 6 and March 7, before a major ICME caused a large FD on March 8. It took two days for the flux to reach the minimum on March 9. As seen in the plot, on March 10 and March 11, the flux magnitude at all rigidities gradually recovered, although they did not reach the level before the FD. There was another FD on March 12 that was caused by a CIR, which is not shown for simplicity. The Maximum Affected Rigidity of this FD according to definitions in Section 3.2 is 33.5 GV. From March 8 to March 11, the normalized fluxes are fit to Equation (1) from 2.97 to 33.5 GV, and the amplitude spectral indices γ are listed in the figure. For this FD, the amplitude spectral index is relatively high during the beginning of decreasing phase on March 8 ($\gamma = 1.03$). On the minimum flux day, March 9, it decreased to $\gamma = 0.23$. This trend agrees with the findings of Alania & Wawrzynczak (2012). However, during the recovery phase, the amplitude spectral index remains constant within the fit errors at a relatively low level. In general, the behaviors of the time evolution of the rigidity spectrum during FDs varies from event to event depending on the complex heliospheric environment. In this paper, for simplicity, the FD rigidity dependence is studied with the normalized rigidity spectrum only on the minimum flux day.

In most cases, the normalized rigidity spectrum on the minimum flux day shows a regular behavior with rigidity: in general, it decreases with decreasing rigidity. Of the 55 ICME FD and 58 CIR FD events, we selected 47 ICME FD and 54 CIR FD events that show a regular rigidity dependence. The other events (i.e., eight ICME FDs and four CIR FDs, marked by "*" in the Appendix) show an irregular normalized rigidity spectra on the minimum flux day. To be more specific, for some events, the normalized rigidity spectrum reaches a minimum around 2 GV, and it then increases with decreasing rigidity. For some other events, there is no clear trend versus rigidity, so that the normalized rigidity spectrum cannot be fitted with a monotonic function. For these events, we also checked that the shape of the normalized rigidity spectrum was not affected by the choice of the reference date. We verified that the shape of the normalized rigidity spectrum remains the same if the normalization is performed with the flux averaged over 3 days before the disturbance date. These events usually have low amplitudes (i.e., less than 5% at all rigidities) and some are happening during the recovery phase of a previous FD. These events are excluded from further analysis in this paper.

Apart from the power-law fit function Equation (1), the regular FD events are analyzed with an exponential fit function. Figures 4(a) and (b) show two examples of the normalized rigidity spectra for an ICME and a CIR FD, respectively, on the minimum flux day along with the fits performed with the

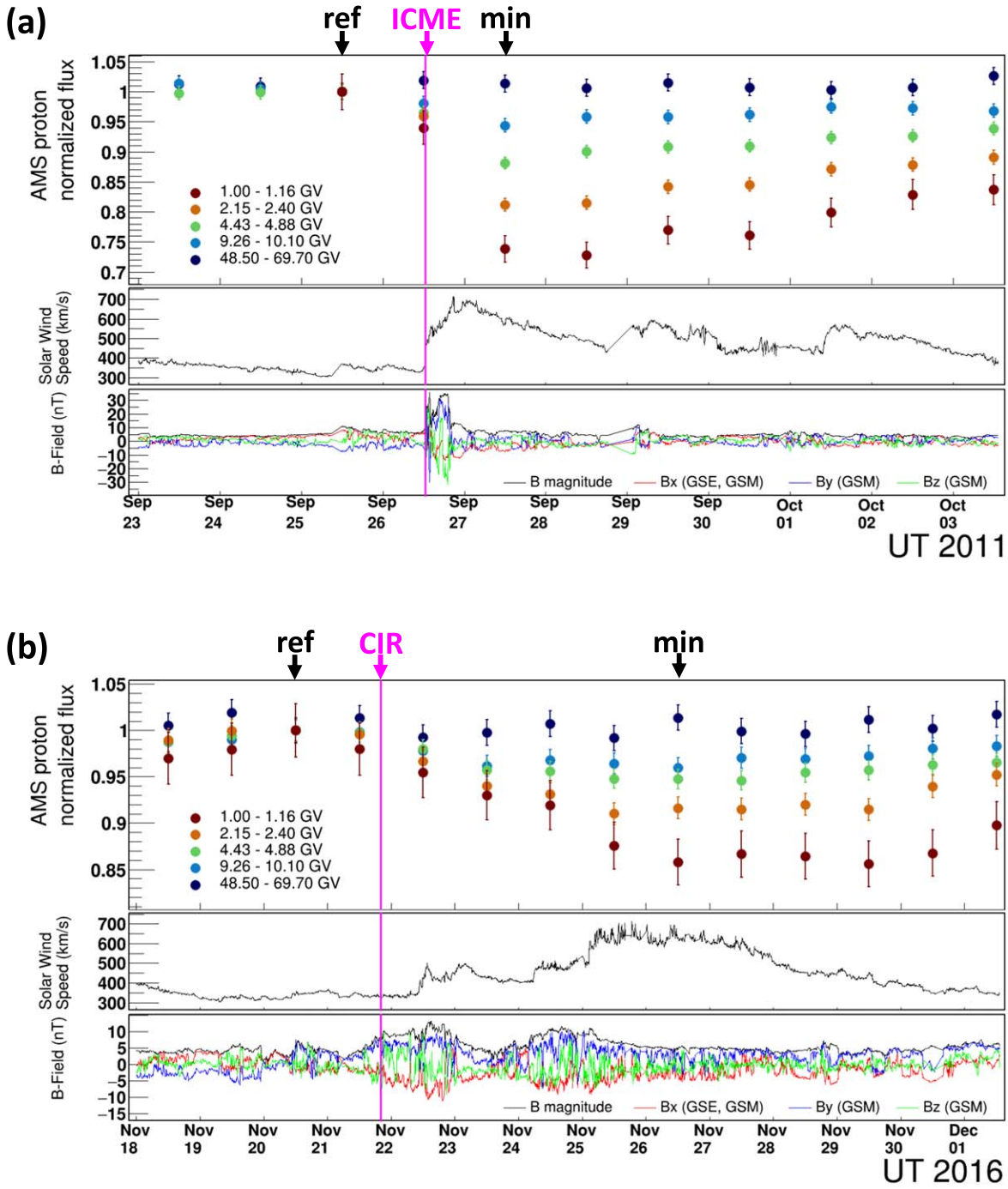

Figure 2. Time profile of the AMS-02 normalized proton flux in five rigidity bins along with the NASA OMNIWeb 5 minute averaged solar wind speed and magnetic field values for (a) an ICME FD on 2011 September 26 and (b) a CIR FD on 2016 November 22. Since the AMS-02 daily proton flux measurement is an average of the flux over 24 hr, the marker position is arbitrarily set at 12:00 pm noon. Vertical-magenta lines mark the arrival time of the ICME or CIR. The ICME arrived on 2011 September 26 at UT 12:34, with speed of 580 km s^{-1}. The CIR arrived on 2016 November 21 at around UT 20:00. The reference date, or date of normalization, is marked with "ref" and the minimum flux day is marked with "min."

exponential and the power-law function. These two FD events are the same ones that are shown in Figure 2. The exponential fit function is:

$$\Phi_{\rm norm} = C - a \cdot e^{-\alpha \cdot R} \quad (2)$$

where C is the asymptotic value , a is a measure of the decrease amplitude at the lowest rigidities, and α gives information on how fast the normalized flux gets close to C as rigidity increases.

To compare the quality of the two fits over all of the events, Figures 5(a) and (b) show the χ^2/ n.d.f. values of the power-law fits versus the exponential fits for ICME and CIR FDs, respectively. In general, the normalized rigidity spectrum fits are better with the exponential function than they are with the power-law function for both ICME and CIR FDs: 77 % of the ICME FD events and 65% of the CIR FD events are better described by the exponential function. Even for those events that are better fit with the power-law function, the χ^2/n.d.f. values of the exponential function are all below 2.5. Overall,

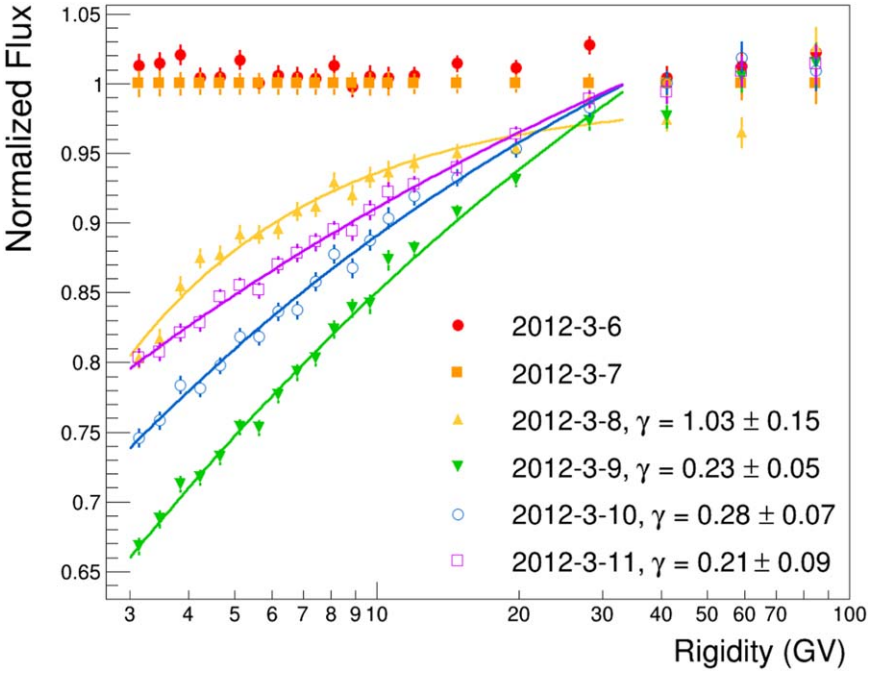

Figure 3. Normalized rigidity spectrum from 2012 March 6 to 2012 March 11. The FD happened on 2012 March 8 due to an ICME on the same day, and reached minimum flux day on 2012 March 9. The fluxes are normalized by the flux on 2012 March 7. From 2012 March 8 to 2012 March 11, the normalized fluxes are fit to Equation (1) from 2.97 to 33.5 GV.

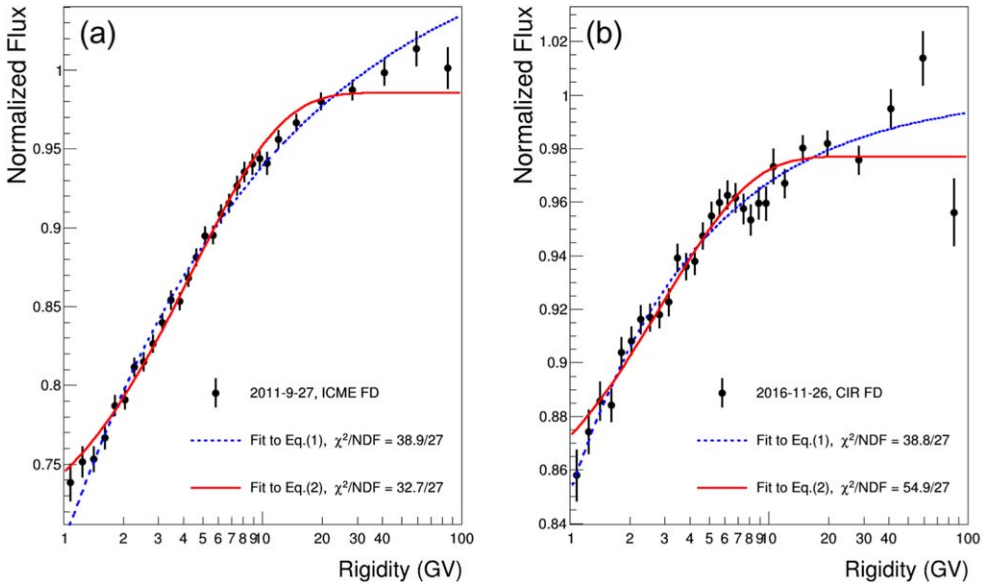

Figure 4. The normalized rigidity spectrum on the minimum flux day for an ICME FD and a CIR FD with power-law fit Equation (1) and exponential fit Equation (2). In (a), the rigidity spectrum on 2011 September 27 is normalized by the spectrum on 2011 September 25, and the χ^2 of Equation (2) is smaller than the χ^2 of Equation (1). In (b), the rigidity spectrum on 2016 November 26 is normalized by the spectrum on 2016 November 20, and the χ^2 of Equation (1) is smaller than the χ^2 of Equation (2).

the χ^2/n.d.f. values of the exponential function for the 47 ICME FD and the 54 CIR FD events are all below 2.5 and centered around 1.2. For some FD events, especially CIR FDs, a power-law function fits better than the exponential function. An example is shown in Figure 4(b). However, for some ICME FD events, the power-law function completely fails and the χ^2/n.d.f. values can reach around 5. For this reason, we will use only the exponential function to study FD characteristics from here on.

The distributions of parameters a, α, and C of the exponential fit function, Equation (2), are shown in Figures 6(a)–(c), respectively. Values of a, α, and C, together with their fit errors, are listed in the Appendix for each fitted event. As shown in the plots, the parameter a ranges from 0.02 to 0.3 for both ICME and CIR FDs, except for the 2012-3-8 ICME FD event where $a > 0.4$. For both ICME and CIR FDs, parameter a is centered around 0.06. The parameter α for ICME FDs ranges from 0.02 to 0.4, while for CIR FDs α

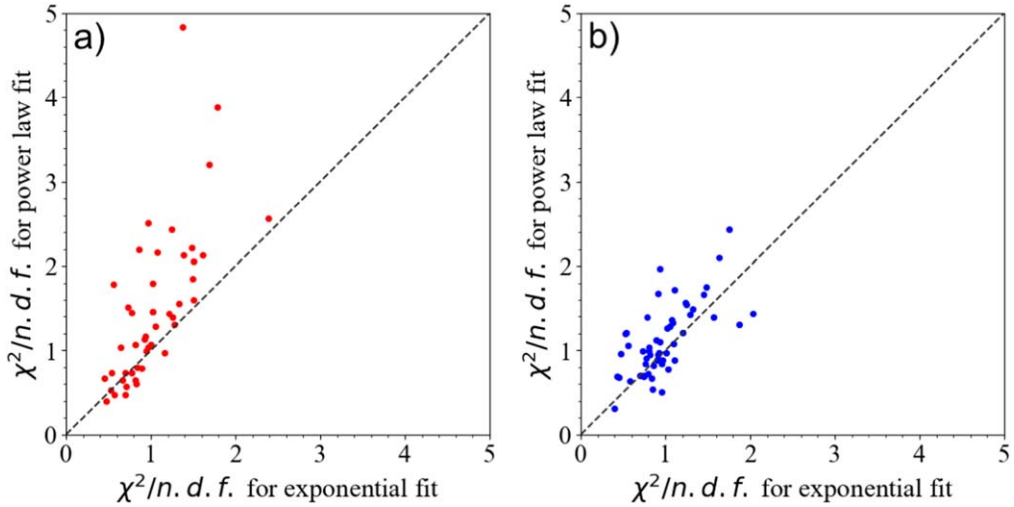

Figure 5. Comparison of the exponential and power-law fits for the FD normalized rigidity spectrum on the minimum flux day for (a) 47 ICME FDs and (b) 54 CIR FDs. Dashed-black lines indicate same χ^2/n.d.f. values.

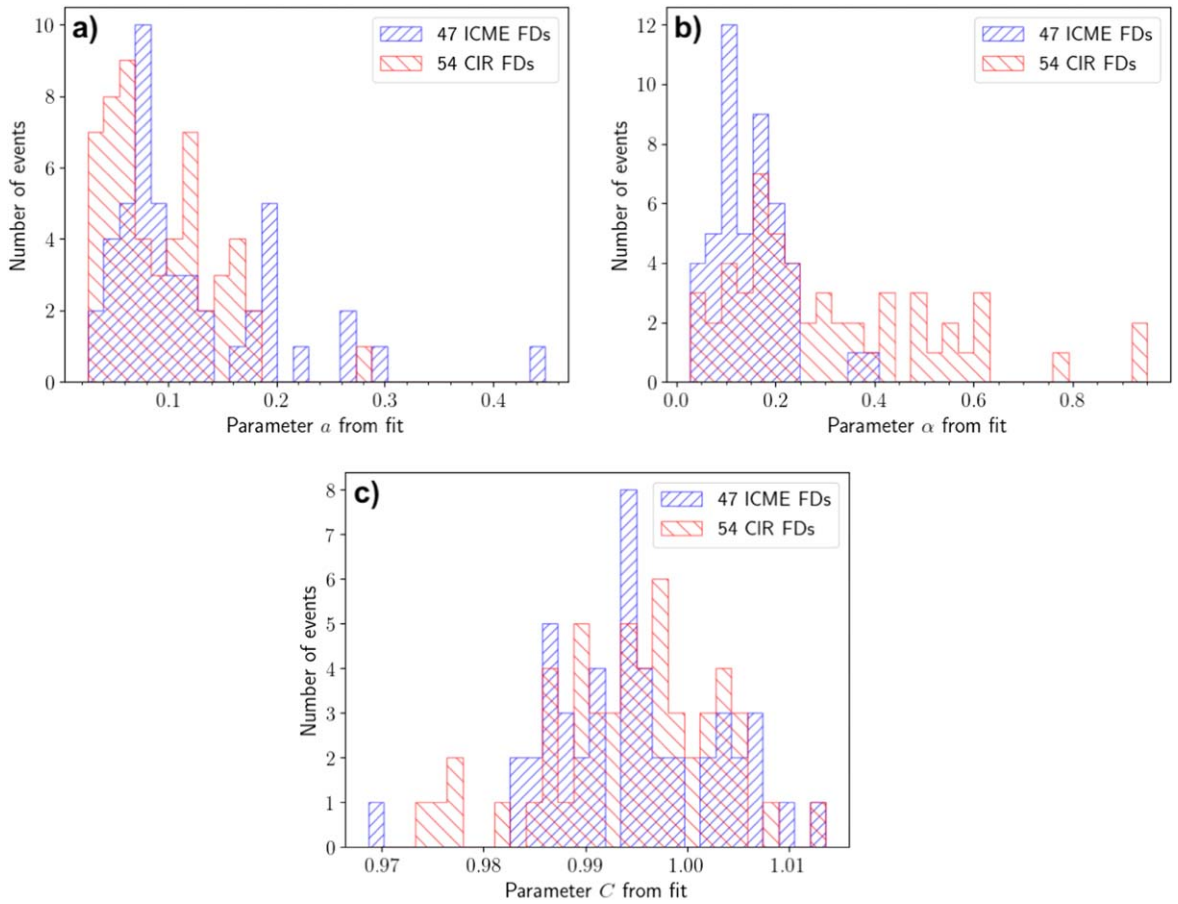

Figure 6. The distribution of exponential function Equation (2) fit parameters for 47 ICME FDs and 54 CIR FDs. (a) a, (b) α, and (c) C.

ranges from 0.02 to 0.95. For both ICME and CIR FDs, most of the time C lies between 0.97 and 1.01.

3.2. FD Amplitude and Maximum Affected Rigidity

With the exponential fit to the normalized rigidity spectrum on the minimum flux day, it is possible to define the FD Amplitude and Maximum Affected Rigidity:

1. The FD Amplitude is defined as the difference between Equation (2)'s asymptotic value (parameter C) and its value at 2 GV (the vertical orange line in Figure 7):

$$\text{FD Amplitude} = C - \Phi_{\text{norm}}|_{\text{at R=2GV}} = a \cdot e^{-\alpha \cdot 2} \quad (3)$$

The rigidity 2 GV is the most representative because Equation (2) generally agrees the best with the data points at 2 GV, especially with respect to lower rigidities. The FD Amplitude is proportional to parameter a.

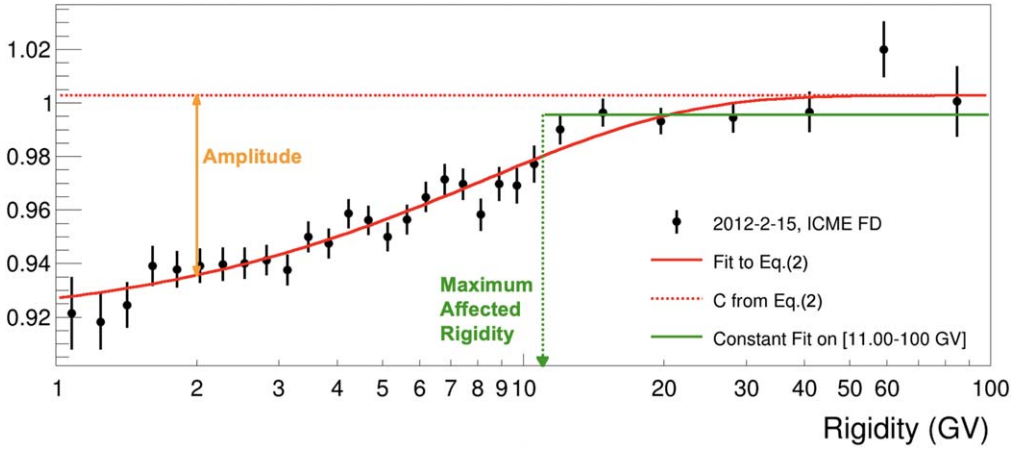

Figure 7. Rigidity spectrum on the minimum flux day, 2012 February 15, of an ICME FD, normalized by the reference spectrum on 2012 February 13, the day before the onset of the ICME on 2012 February 14. The red line is the exponential fit and the red-dashed line is the asymptotic value of the fit. The length of the orange line between the fit at 2 GV and the asymptotic value shows the FD Amplitude. The green line is the constant fit from 11 to 100 GV. In this rigidity range, the χ^2 of the constant fit is smaller than that of the exponential fit. The green-dashed arrow points to the Maximum Affected Rigidity at 11 GV for this event.

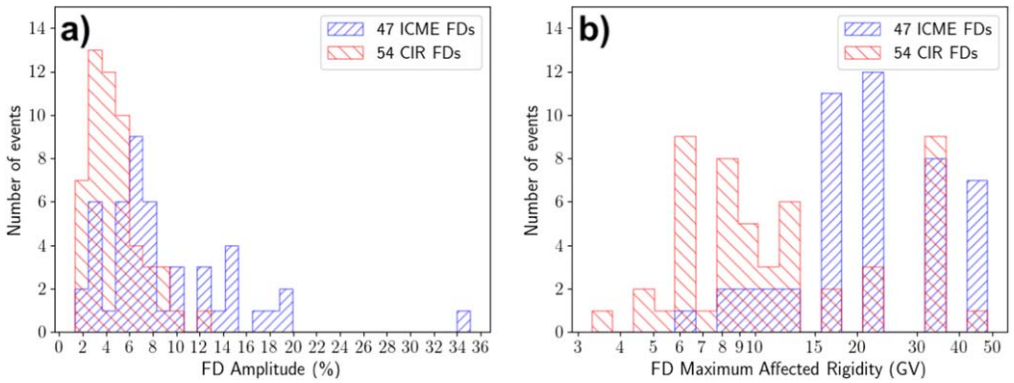

Figure 8. The distributions of FD characteristics for 47 ICME FDs and 54 CIR FDs. (a) FD Amplitude (%), and (b) Maximum Affected Rigidity (GV).

2. The Maximum Affected Rigidity (MAR) is the rigidity up to which FD effects are still significant. Above the Maximum Affected Rigidity, the normalized flux is flat and can be fitted with a constant. The Maximum Affected Rigidity is obtained by comparing (1) the fit of the rigidity dependence performed with Equation (2) on the whole rigidity range with (2) a constant fit performed on various rigidity ranges where the minimum fitted rigidity progressively increases. The Maximum Affected Rigidity is defined as the minimum (fitted) rigidity where the χ^2 of the constant fit is smaller than the χ^2 of the exponential fit (computed for the same rigidity range).

Figure 7 shows an example of this procedure. The red solid line is the exponential fit Equation (2) fit to normalized flux from 1 to 100 GV:

$$\Phi_{\rm norm} = 1.003\text{–}0.085 \cdot e^{-0.121 \cdot R} \quad (4)$$

The green-solid line is a constant fit performed from 11 to 100 GV. In this rigidity interval, the χ^2 of the constant fit is 7.0, which is smaller than the χ^2 of Equation (4) (i.e., 8.7). When the fit range starts below 11 GV (e.g., when fitting a constant from 10.1 GV to 100 GV), the χ^2 of the constant fit is larger than the χ^2 of Equation (4) in the rigidity range from 10.1 GV to 100 GV. Thus, 11 GV is the Maximum Affected Rigidity for this FD. Note that with this method, the Maximum Affected Rigidity is always aligned with the lower edge of one of the AMS rigidity bins.

The FD Amplitude and Maximum Affected Rigidity distribution for both ICME FDs and CIR FDs are shown in Figures 8(a) and (b), respectively. (Exact FD Amplitude and Maximum Affected Rigidity values are listed in the Appendix). The FD Amplitudes of the CIR FDs range from ∼1% to ∼12%, centered around 4%, while the ICME FDs are distributed between ∼2% and ∼20%, with one extreme case of a FD Amplitude of ∼35% (March 8, 2012). Thus, the FD Amplitudes of the CIR FDs are generally much smaller than the ICME FD ones. This result is consistent with previous studies performed by Lockwood (1971) and Raghav et al. (2020), and so on.

The Maximum Affected Rigidity of the CIR FDs ranges from ∼3 to ∼50 GV, while the Maximum Affected Rigidity of ICME FDs ranges from ∼6 to ∼50 GV. In general, ICME FDs have larger Maximum Affected Rigidity than CIR FDs.

As shown in Figures 9(a) and (b), there is no correlation between FD Amplitude and Maximum Affected Rigidity for ICME FDs: the correlation coefficient is 0.13, with a 95% confidence interval of [−0.16, 0.39], which is consistent with zero. For CIR FDs, there is only a weak correlation between FD Amplitude and Maximum Affected Rigidity because the correlation coefficient is 0.42 with a 95% confidence interval of [0.18, 0.61]. This implies that the processes driving the

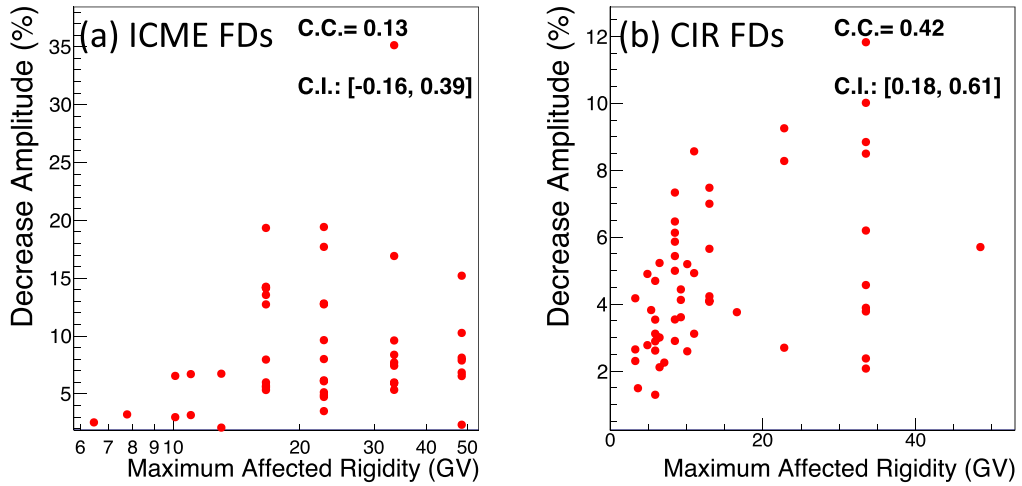

Figure 9. The correlation between FD Amplitude and Maximum Affected Rigidity for (a) 47 ICME FD events and (b) 54 CIR FD events. "C.C." denotes correlation coefficients; "C.I." denotes the corresponding 95% confidence interval.

Table 1
Correlation Coefficients Among Normalized Rigidity Spectrum Fit Parameters and FD Properties

ICME FDs	FD Amplitude	MAR	a	α
FD Amplitude	1	0.13, [−0.16, 0.39]	**0.98, [0.97, 0.99]**	−0.07, [−0.34, 0.21]
MAR	⋯	1	0.01, [−0.27, 0.29]	**−0.68, [−0.81, −0.50]**
a	⋯	⋯	1	0.08, [−0.21, 0.35]
α	⋯	⋯	⋯	1
CIR FDs	**FD Amplitude**	**MAR**	a	α
FD Amplitude	1	*0.42, [0.18, 0.61]*	**0.55, [0.34, 0.71]**	−0.26, [−0.48, 0.01]
MAR	⋯	1	−0.16, [−0.40, 0.11]	**−0.62, [−0.76, −0.42]**
a	⋯	⋯	1	**0.61, [0.41, 0.75]**
α	⋯	⋯	⋯	1

Note. The 95% confidence intervals are listed after the correlation coefficients (C.C.). Strong and moderate correlations (C.C. $\geqslant 0.5$) are marked in bold, while weak correlations (C.C. < 0.5) are marked in italic. The other correlations are consistent with zero within the 95% confidence interval.

amplitude of FDs are more rigidity-dependent for CIRs than for ICMEs.

The correlation coefficients among fit parameters a, α, FD Amplitude, and Maximum Affected Rigidity are summarized in Table 1. For ICME FDs, parameter a has a strong correlation (0.98) with the FD Amplitude, while the correlation (0.55) is only moderate for CIR FDs. This is expected because the FD Amplitude and a are related by Equation (2). The Maximum Affected Rigidity has a moderate correlation with parameter α for both ICME FDs (−0.68) and CIR FDs (−0.62), but no correlation with parameter a. This is also expected because α controls the rate at which the flux decrease magnitude goes down as the rigidity goes up.

4. Correlation Between FD Properties and Solar Wind Parameters

For the 47 ICME FD and the 54 CIR FD events that we have considered so far, we investigated the correlation between selected solar wind parameters and both FD Amplitude and Maximum Affected Rigidity. The correlation coefficients (C.C.) and their corresponding 95% confidence intervals (C.I.) are listed in Table 2.

The ICME-speed data are taken from Richardson & Cane (2010). When a FD is caused by a cluster of two to four sequential ICMEs, the ICME speed that is used for the correlation is the largest. The other correlation quantities are based on 5 minute averaged solar wind data and the hourly averaged Disturbance Storm-Time (Dst) index taken from NASA OMNIWeb. The "Maximum" and "Minimum" values are found to be within the time interval from the beginning of the disturbance date to the end of the minimum flux day. The solar wind parameter "increase" is the difference between (1) the maximum value during the period from the disturbance date to the minimum flux day and (2) the average value during the day before the disturbance. Note that the solar wind speed can reach a maximum before the minimum flux day.

For the 47 ICME FDs, there is a moderate correlation between the FD Amplitude and minimum Dst index. There is also a moderate correlation between FD Amplitude and some of the solar wind parameters during the ICME events (i.e., maximum magnetic field magnitude, maximum temperature, maximum pressure, increase in solar wind speed, increase in pressure, and increase in temperature). Maximum plasma Beta, Alfvén Mach number, and magnetosonic Mach number all showed no correlation with the ICME FD Amplitude. Figure 10 shows for the 47 ICME FD events the correlations between the FD Amplitude and the four of the most correlated quantities: (a) Temperature Increase, (b) Solar Wind Speed Increase, (c) Maximum Magnetic Field and (d) Maximum Pressure. The foregoing results are in agreement with Light et al. (2020), except that the correlation with maximum

Table 2
Correlations between FD Properties and Solar Wind Parameters, for ICME FDs and CIR FDs

Solar Wind Parameters	ICME FD Amplitude		ICME FD MAR		CIR FD Amplitude		CIR FD MAR	
	C.C.	C.I.	C.C.	C.I.	C.C.	C.I.	C.C.	C.I.
Temperature increase	**0.60**	**[0.38, 0.75]**	0.04	[−0.24, 0.31]	0.01	[−0.25, 0.27]	*0.27*	*[0.01, 0.49]*
Maximum temperature	**0.58**	**[0.36, 0.74]**	0.02	[−0.26, 0.30]	0.04	[−0.22, 0.30]	0.25	[−0.01, 0.48]
Solar wind speed increase	**0.55**	**[0.32, 0.72]**	−0.01	[−0.29, 0.27]	−0.10	[−0.35, 0.17]	0.17	[−0.10, 0.41]
Maximum magnetic field	**0.55**	**[0.32, 0.72]**	0.19	[−0.10, 0.44]	−0.02	[−0.28, 0.24]	0.23	[−0.03, 0.46]
Maximum pressure	**0.53**	**[0.29, 0.70]**	0.19	[−0.09, 0.45]	−0.05	[−0.30, 0.22]	0.07	[−0.20, 0.32]
Minimum Dst index	**−0.51**	**[−0.69, −0.27]**	−0.15	[−0.41, 0.14]	0.01	[−0.25, 0.27]	−0.26	[−0.48, 0.01]
Pressure increase	**0.50**	**[0.26, 0.68]**	0.20	[−0.08, 0.45]	−0.08	[−0.33, 0.19]	0.05	[−0.21, 0.31]
Minimum B_z value	*−0.47*	*[-0.66, -0.22]*	−0.25	[−0.49, 0.03]	0.04	[−0.22, 0.30]	−0.17	[−0.41,0.09]
ICME speed	*0.41*	*[0.15, 0.62]*	−0.06	[−0.33, 0.22]	…	…	…	…
Maximum solar wind speed	*0.40*	*[0.13, 0.61]*	−0.05	[−0.32, 0.23]	−0.11	[−0.36, 0.15]	0.04	[−0.22, 0.30]
Maximum proton density	0.25	[−0.03, 0.49]	0.20	[−0.08, 0.46]	−0.23	[−0.46, 0.04]	0.00	[−0.26, 0.26]
Proton density increase	0.20	[−0.08, 0.46]	0.22	[−0.06, 0.47]	−0.24	[−0.47, 0.02]	−0.03	[−0.29, 0.24]
Magnetosonic Mach number increase	0.05	[−0.23, 0.32]	−0.17	[−0.42, 0.12]	−0.02	[−0.28, 0.24]	0.05	[−0.22, 0.30]
Maximum magnetosonic Mach number	0.02	[−0.26, 0.30]	−0.12	[−0.38, 0.17]	*−0.27*	*[-0.50, -0.01]*	−0.10	[−0.35, 0.17]
Maximum Alfvén Mach number	0.00	[−0.28, 0.28]	0.08	[−0.20, 0.35]	*−0.29*	*[−0.52, −0.04]*	−0.21	[−0.44, 0.06]
Alfvén Mach number increase	0.00	[−0.28, 0.28]	0.07	[−0.21, 0.35]	*−0.26*	*[−0.49, 0.00]*	−0.20	[−0.44, 0.06]
Maximum plasma beta	0.00	[−0.28, 0.28]	0.07	[−0.21, 0.34]	−0.24	[−0.47, 0.02]	−0.15	[−0.39, 0.12]

Note."C.C." denotes correlation coefficients, and "C.I." denotes their 95% confidence intervals. Solar wind parameters were derived from NASA OMNIWeb. Moderate correlations (C.C. $\geqslant 0.5$) are marked in bold, while weak correlations (C.C. < 0.5) are marked in italic. The rest of the correlations are consistent with zero within the 95% confidence interval.

pressure in this paper is found to be moderate instead of weak; the correlation with ICME speed and maximum solar wind speed is weaker than Light et al. (2020), which can be explained by (1) the different sample of events and (2) the fact that the daily averaged AMS fluxes have a smaller relative variation than NM hourly count rates before and during FDs.

Note that even without the extreme ICME FD event on 2012 March 8, the correlation coefficients in Table 2 remain within their 95% confidence intervals. This means that any correlation, when statistically significant, is not driven by this event.

While the correlations between ICME FD Amplitude and solar wind parameters have been extensively researched in previous studies (see, e.g., Light et al. 2020; Papaioannou et al. 2020 and references therein), the corresponding correlations for CIR FDs have received comparatively less attention and are not yet fully understood. We found that there is no correlation between the CIR FD Amplitude and any of the following: maximum solar wind speed, solar wind speed increase, and maximum magnetic field magnitude. This agrees with Kallaya & Yeeram (2021), whose findings suggest that these correlations are weak from 2008 to 2011 (i.e., during negative solar magnetic polarity) and that there is no consistent relationship from 2015 to 2016 (i.e., during positive solar magnetic polarity). Among all of the selected solar wind parameters, we found only very weak correlations between the CIR FD Amplitude and each of the following: the maximum magnetosonic Mach number, maximum Alfvén Mach number, and Alfvén Mach number increase.The other correlations between the CIR FD Amplitude and solar wind parameters are all negligible.

We also investigated the relationship between the Maximum Affected Rigidity of FDs and solar wind parameters. As far as the available literature suggests, this is the first time that such studies have been done. However, our analysis reveals that the correlations between these parameters and the Maximum Affected Rigidity, for both ICME FDs and CIR FDs, have correlation coefficients that are consistent with zero at the 95% confidence level (with one exception: the very weak correlation between temperature increase and the Maximum Affected Rigidity of CIR FDs). These findings suggest that other factors may be more important in determining the Maximum Affected Rigidity of FDs. Further research is needed to identify these factors and to better understand the complex processes that are involved in FDs. Studies similar to ours could be done using cosmic-ray data from other satellites or NMs with a wide range of different cutoff rigidities, which is beyond the scope of this paper.

Although the fit parameter α of Equation (2) describes the steepness of the decrease amplitude in the normalized rigidity spectrum, no correlation was found between it and any solar wind quantities for either ICME or CIR FD events, except for one very weak correlation (0.28) between α and Magnetosonic mach number increase for CIR FDs. For ICME FDs, because the correlation between a and FD Amplitude is nearly 1 (0.98), parameter a has correlations with the solar wind parameters that are very similar to those of the FD Amplitude. For CIR FDs, there is no correlation between a and solar wind parameters except for very weak correlations with the Magnetic Field increase (−0.28) and Maximum Proton Density (−0.27).

5. Conclusion

We analyzed the daily AMS-02 cosmic-ray proton flux measured from 2011 May 20 to 2019 October 29 and identified 142 FD events. We categorized them by related solar wind transients: 55 were attributed to pure ICMEs and 58 were attributed to pure CIRs.

We selected 47 ICME FD events and 54 CIR FD events with a clear trend in rigidity and fitted the normalized rigidity spectrum on the minimum flux day with two parametric functions versus rigidity: an exponential function and a power-law function. For both ICME FDs and CIR FDs, the exponential function fits better than the power-law function in general.

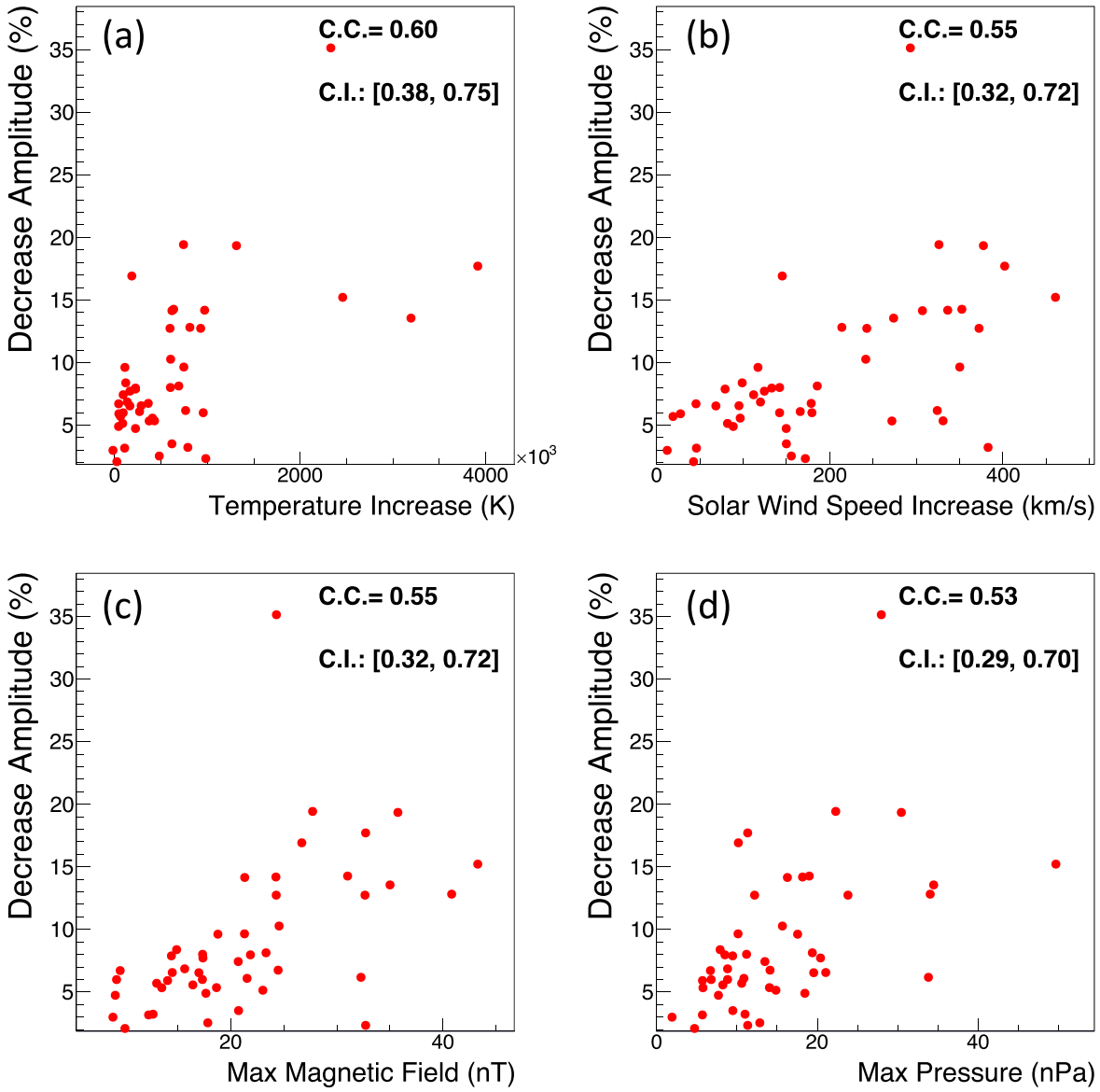

Figure 10. Correlation between FD Amplitude and (a) Temperature Increase, (b) Solar Wind Speed Increase, (c) Maximum Magnetic Field Magnitude, (d) Maximum Pressure for 47 ICME FD events.

We defined the FD Amplitude and the Maximum Affected Rigidity, and we correlated them with a number of solar wind parameters. We found that there is a moderate correlation between the FD Amplitude of the ICME FDs and several solar wind parameters, but there is no correlation between the Maximum Affected Rigidity of the ICME FDs and any of the solar wind parameters. We also found that for the CIR FDs events, there is little to no correlation between any of the solar wind parameters and either the FD Amplitude or the Maximum Affected Rigidity.

There is only a weak correlation between FD Amplitude and Maximum Affected Rigidity for CIR FDs and no correlation for ICME FDs.

This work has been supported by NASA Future Investigators in NASA Earth and Space Science and Technology (FINESST 80NSSC21K1392), NASA Living with the Star (LWS 80NSSC20K1819), National Science Foundation Career grant (NSF AGS-1455202); and Wyle Laboratories, Light et al. Inc., grant (NAS 9-02078). We acknowledge the use of NASA/GSFC's Space Physics Data Facility's OMNIWeb service, and OMNI data. This work utilizes the HSS catalog issued by G. Mariş Muntean, D. Beşliu-Ionescu, V. Dobrică managed by the Institute of Geodynamics of the Romanian Academy.

Appendix
AMS FD Event List

The AMS FD events are listed in Table 3, along with FD Amplitude and Maximum Affected Rigidity, which are defined in Section 3.2, and parameters a, α, and C of Equation (2) fitted to the normalized rigidity spectrum of each FD. Every FD event associated with ICME is also in the near-Earth ICME catalog of Richardson & Cane (2010). All of the events in Table 3 are also included in the IZMIRAN database of the catalog of the Forbush-effects and interplanetary disturbances[4]. FDs marked with star "*" are not analyzed with fitting functions. Note that a single

[4] http://spaceweather.izmiran.ru/eng/dbs.html

Table 3
List of FD Events Derived with AMS Daily Proton Data

No.	FD start	Solar Activity	Minimum Flux Day	a	α	C	FD Amplitude (%)	MAR (GV)
1	2011-06-11	CIR 2011-06-11	2011-06-11	0.071 ± 0.008	0.205 ± 0.039	0.995 ± 0.004	4.7 ± 0.5	5.9
2	2011-06-17*	ICME 2011-06-17						
3	2011-06-23	CIR 2011-06-20	2011-06-24	0.114 ± 0.007	0.162 ± 0.027	0.997 ± 0.005	8.3 ± 0.6	22.8
4	2011-07-11	CIR 2011-07-09	2011-07-12	0.060 ± 0.019	0.026 ± 0.015	1.014 ± 0.021	5.7 ± 2.0	48.5
5	2011-07-21	CIR 2011-07-19	2011-07-21	0.104 ± 0.012	0.305 ± 0.056	0.993 ± 0.003	5.7 ± 0.4	13
6	2011-08-06	ICME 2011-08-04	2011-08-06	0.190 ± 0.006	0.168 ± 0.013	0.994 ± 0.004	13.6 ± 0.4	16.6
		ICME 2011-08-05						
7	2011-09-10	ICME 2011-09-08	2011-09-10	0.098 ± 0.008	0.096 ± 0.025	1.005 ± 0.007	8.1 ± 0.7	48.5
		ICME 2011-09-09						
8	2011-09-17	ICME 2011-09-16	2011-09-18	0.101 ± 0.007	0.218 ± 0.029	1.001 ± 0.003	6.6 ± 0.4	10.1
		ICME 2011-09-17						
		ICME 2011-09-18						
9	2011-09-26	ICME 2011-09-26	2011-09-27	0.300 ± 0.006	0.219 ± 0.010	0.986 ± 0.003	19.3 ± 0.4	16.6
10	2011-10-25	ICME 2011-10-24	2011-10-25	0.122 ± 0.005	0.087 ± 0.010	0.989 ± 0.005	10.3 ± 0.5	48.5
11	2011-11-29	ICME 2011-11-28	2011-11-29	0.051 ± 0.012	0.346 ± 0.125	0.994 ± 0.003	2.5 ± 0.4	6.47
12	2012-01-22	ICME 2012-01-21						
		ICME 2012-01-22						
		CIR 2012-01-22						
13	2012-01-25	CIR 2012-01-24	2012-01-25	0.063 ± 0.010	0.288 ± 0.076	0.996 ± 0.003	3.5 ± 0.4	5.9
14	2012-02-01	⋯						
15	2012-02-15	ICME 2012-02-14	2012-02-15	0.085 ± 0.005	0.121 ± 0.018	1.003 ± 0.004	6.7 ± 0.4	11
16	2012-02-27	ICME 2012-02-26	2012-02-28	0.093 ± 0.007	0.054 ± 0.009	1.006 ± 0.007	8.4 ± 0.7	33.5
17	2012-03-08	ICME 2012-03-08	2012-03-09	0.448 ± 0.008	0.121 ± 0.005	0.986 ± 0.005	35.1 ± 0.5	33.5
18	2012-03-12	CIR 2012-03-12	2012-03-12	0.144 ± 0.007	0.259 ± 0.023	1.000 ± 0.003	8.6 ± 0.3	11
19	2012-04-05	⋯						
20	2012-04-25	ICME 2012-04-25	2012-04-26	0.053 ± 0.007	0.247 ± 0.054	0.984 ± 0.003	3.2 ± 0.3	7.76
21	2012-05-31	⋯						
22	2012-06-17	ICME 2012-06-16	2012-06-18	0.184 ± 0.007	0.181 ± 0.017	0.994 ± 0.005	12.8 ± 0.5	22.8
23	2012-07-15	ICME 2012-07-14	2012-07-15	0.273 ± 0.005	0.170 ± 0.008	0.991 ± 0.004	19.4 ± 0.4	22.8
24	2012-07-19	⋯						
25	2012-09-03	ICME 2012-09-03	2012-09-05	0.189 ± 0.006	0.196 ± 0.014	0.983 ± 0.003	12.7 ± 0.4	16.6
		ICME 2012-09-04						
26	2012-10-01	ICME 2012-09-30	2012-10-02	0.119 ± 0.006	0.200 ± 0.020	0.996 ± 0.003	8.0 ± 0.4	16.6
		ICME 2012-09-30						
27	2012-10-08	ICME 2012-10-08						
		CIR 2012-10-08						
28	2012-11-13	ICME 2012-11-12	2012-11-13	0.100 ± 0.006	0.196 ± 0.022	0.995 ± 0.003	6.7 ± 0.4	13
29	2012-11-24	ICME 2012-11-23	2012-11-25	0.080 ± 0.007	0.079 ± 0.022	0.998 ± 0.008	6.9 ± 0.8	48.5
30	2013-01-17	ICME 2013-01-17	2013-01-19	0.077 ± 0.006	0.079 ± 0.017	1.009 ± 0.007	6.5 ± 0.7	48.5
		ICME 2013-01-18						
31	2013-02-17*	ICME 2013-02-16						
32	2013-03-15	⋯						
33	2013-03-17	ICME 2013-03-17	2013-03-19	0.198 ± 0.005	0.167 ± 0.011	0.989 ± 0.004	14.1 ± 0.4	16.6
34	2013-04-14	ICME 2013-04-13	2013-04-15	0.095 ± 0.006	0.091 ± 0.017	0.988 ± 0.005	7.9 ± 0.5	48.5
35	2013-05-06	CIR 2013-05-05	2013-05-08	0.111 ± 0.007	0.230 ± 0.026	0.994 ± 0.003	7.0 ± 0.3	13
36	2013-05-16	⋯						
37	2013-05-18	⋯						
38	2013-05-21	⋯						
39	2013-06-01	CIR 2013-05-31	2013-06-02	0.029 ± 0.006	0.163 ± 0.092	1.004 ± 0.004	2.1 ± 0.4	33.5
40	2013-06-07	ICME 2013-06-06	2013-06-07	0.070 ± 0.005	0.101 ± 0.020	1.006 ± 0.005	5.7 ± 0.5	16.6
41	2013-06-23	CIR 2013-06-19	2013-06-24	0.046 ± 0.009	0.055 ± 0.022	0.987 ± 0.009	4.1 ± 0.9	13
42	2013-07-10	⋯						
43	2013-07-13	ICME 2013-07-12	2013-07-13	0.068 ± 0.005	0.100 ± 0.018	1.006 ± 0.004	5.6 ± 0.5	16.6
44	2013-08-24	ICME 2013-08-24	2013-08-25	0.065 ± 0.018	0.391 ± 0.138	0.988 ± 0.003	3.0 ± 0.4	10.1
45	2013-09-03	⋯						
46	2013-10-02	ICME 2013-10-02	2013-10-02	0.079 ± 0.005	0.124 ± 0.025	0.995 ± 0.005	6.2 ± 0.5	22.8
47	2013-10-15	CIR 2013-10-14	2013-10-16	0.052 ± 0.007	0.065 ± 0.026	1.004 ± 0.007	4.6 ± 0.7	33.5
48	2013-10-30	⋯						
49	2013-11-11	ICME 2013-11-08						
		ICME 2013-11-11						
		CIR 2013-11-07						
50	2013-11-27	⋯						
51	2013-12-01	ICME 2013-11-30	2013-12-02	0.067 ± 0.005	0.114 ± 0.023	0.994 ± 0.004	5.3 ± 0.4	16.6
52	2013-12-15	ICME 2013-12-15	2013-12-15	0.074 ± 0.006	0.109 ± 0.025	0.994 ± 0.006	6.0 ± 0.6	33.5

Table 3
(Continued)

No.	FD start	Solar Activity	Minimum Flux Day	a	α	C	FD Amplitude (%)	MAR (GV)
53	2014-01-08	⋯						
54	2014-01-10	⋯						
55	2014-02-04	⋯						
56	2014-02-16	ICME 2014-02-15	2014-02-16	0.096 ± 0.005	0.109 ± 0.017	0.999 ± 0.005	7.7 ± 0.5	33.5
57	2014-02-20	ICME 2014-02-19	2014-02-21	0.071 ± 0.005	0.144 ± 0.030	0.992 ± 0.004	5.3 ± 0.4	33.5
		ICME2014-02-20						
58	2014-02-28	CIR 2014-02-28	2014-03-01	0.120 ± 0.006	0.091 ± 0.016	0.999 ± 0.006	10.0 ± 0.5	33.5
59	2014-04-06	ICME 2014-04-05	2014-04-06	0.069 ± 0.006	0.173 ± 0.035	0.991 ± 0.004	4.9 ± 0.4	22.8
60	2014-04-18	ICME 2014-04-18	2014-04-20	0.133 ± 0.010	0.162 ± 0.022	0.984 ± 0.004	9.6 ± 0.5	22.8
		ICME 2014-04-19						
		ICME 2014-04-20						
61	2014-05-23	CIR 2014-05-22	2014-05-24	0.131 ± 0.008	0.217 ± 0.025	0.993 ± 0.003	8.5 ± 0.4	33.5
62	2014-06-08*	ICME 2014-06-07						
63	2014-06-17	CIR 2014-06-17	2014-06-20	0.169 ± 0.007	0.178 ± 0.017	0.990 ± 0.004	11.8 ± 0.5	33.5
64	2014-07-15	CIR 2014-07-15	2014-07-15	0.042 ± 0.006	0.171 ± 0.051	0.994 ± 0.003	3.0 ± 0.4	6.47
65	2014-09-06	⋯						
66	2014-09-12	ICME 2014-09-12	2014-09-13	0.186 ± 0.008	0.132 ± 0.011	0.987 ± 0.004	14.3 ± 0.5	16.6
67	2014-12-02	CIR 2014-11-30	2014-12-02	0.114 ± 0.005	0.125 ± 0.013	0.986 ± 0.004	8.8 ± 0.4	33.5
68	2014-12-05	⋯						
69	2014-12-21	ICME 2014-12-21	2014-12-22	0.200 ± 0.005	0.083 ± 0.006	0.995 ± 0.005	16.9 ± 0.5	33.5
70	2014-12-23	CIR 2014-12-23	2014-12-24	0.084 ± 0.005	0.153 ± 0.024	1.000 ± 0.004	6.2 ± 0.4	33.5
71	2014-12-29	CIR 2014-12-28	2015-01-01	0.280 ± 0.052	0.951 ± 0.105	0.997 ± 0.002	4.2 ± 0.3	3.29
72	2015-03-16	ICME 2015-03-16	2015-03-18	0.184 ± 0.006	0.184 ± 0.013	0.984 ± 0.003	12.7 ± 0.4	22.8
		ICME 2015-03-17						
73	2015-04-01	ICME 2015-03-31						
		CIR 2015-03-31						
74	2015-04-10	ICME 2015-04-09	2015-04-10	0.090 ± 0.005	0.095 ± 0.017	1.007 ± 0.005	7.4 ± 0.5	33.5
		ICME 2015-04-10						
75	2015-05-06	ICME 2015-05-06	2015-05-07	0.130 ± 0.005	0.151 ± 0.015	0.996 ± 0.004	9.6 ± 0.4	33.5
76	2015-06-22	ICME 2015-06-22	2015-06-23	0.168 ± 0.007	0.050 ± 0.005	0.990 ± 0.008	15.2 ± 0.7	48.5
77	2015-06-25	ICME 2015-06-24	2015-06-25	0.074 ± 0.005	0.106 ± 0.019	1.012 ± 0.004	6.0 ± 0.5	16.6
78	2015-07-13*	ICME 2015-07-13						
79	2015-08-26	ICME 2015-08-26	2015-08-27	0.065 ± 0.008	0.046 ± 0.011	1.004 ± 0.008	5.9 ± 0.8	33.5
80	2015-09-08	ICME 2015-09-07	2015-09-08	0.075 ± 0.005	0.106 ± 0.017	0.998 ± 0.004	6.1 ± 0.4	22.8
81	2015-11-04	ICME 2015-11-04	2015-11-04	0.072 ± 0.007	0.212 ± 0.040	0.996 ± 0.003	4.7 ± 0.4	22.8
82	2015-11-07	ICME 2015-11-06	2015-11-07	0.046 ± 0.005	0.133 ± 0.045	0.991 ± 0.004	3.5 ± 0.4	22.8
83	2015-11-10	CIR 2015-11-08	2015-11-11	0.174 ± 0.050	0.941 ± 0.162	1.005 ± 0.002	2.6 ± 0.3	3.29
84	2015-12-20*	ICME 2015-12-19						
85	2015-12-31	ICME 2015-12-31	2016-01-01	0.115 ± 0.005	0.179 ± 0.020	0.987 ± 0.003	8.0 ± 0.4	22.8
86	2016-02-04	CIR 2016-02-02	2016-02-06	0.117 ± 0.024	0.597 ± 0.110	0.990 ± 0.002	3.5 ± 0.3	8.48
87	2016-02-28	CIR 2016-02-25	2016-02-28	0.146 ± 0.016	0.493 ± 0.057	0.982 ± 0.002	5.4 ± 0.3	8.48
88	2016-03-06	ICME 2016-03-05						
		CIR 2016-03-06						
89	2016-03-25	CIR 2016-03-21	2016-03-25	0.120 ± 0.015	0.437 ± 0.063	0.995 ± 0.002	5.0 ± 0.3	8.48
90	2016-04-22	CIR 2016-04-20	2016-04-22	0.159 ± 0.019	0.555 ± 0.063	0.990 ± 0.002	5.2 ± 0.3	6.47
91	2016-06-06	CIR 2016-06-04	2016-06-06	0.062 ± 0.009	0.250 ± 0.069	0.997 ± 0.004	3.8 ± 0.4	16.6
92	2016-06-14	CIR 2016-06-14	2016-06-17	0.184 ± 0.020	0.549 ± 0.061	0.978 ± 0.002	6.1 ± 0.3	8.48
93	2016-06-23*	CIR 2016-06-22						
94	2016-07-08	CIR 2016-07-06	2016-07-11	0.091 ± 0.006	0.222 ± 0.028	0.986 ± 0.003	5.9 ± 0.3	8.48
95	2016-07-12	CIR 2016-07-11	2016-07-14	0.164 ± 0.020	0.603 ± 0.068	0.985 ± 0.002	4.9 ± 0.3	4.88
96	2016-07-20*	ICME 2016-07-19						
97	2016-08-03	ICME 2016-08-02						
		CIR 2016-08-02						
98	2016-08-07	⋯						
99	2016-08-31	CIR 2016-08-29	2016-09-04	0.107 ± 0.011	0.362 ± 0.055	0.976 ± 0.002	5.2 ± 0.3	10.1
100	2016-09-18*	CIR 2016-09-17						
101	2016-09-28	CIR 2016-09-25	2016-09-30	0.105 ± 0.021	0.608 ± 0.108	0.992 ± 0.002	3.1 ± 0.3	5.9
102	2016-10-13*	ICME 2016-10-12						
103	2016-10-15	⋯						
104	2016-10-25	CIR 2016-10-22	2016-10-29	0.076 ± 0.022	0.605 ± 0.168	0.974 ± 0.002	2.3 ± 0.3	7.09
105	2016-11-22	CIR 2016-11-21	2016-11-26	0.146 ± 0.009	0.335 ± 0.033	0.977 ± 0.002	7.5 ± 0.3	13
106	2016-12-19	⋯						
107	2017-02-17	CIR 2017-02-15	2017-02-18	0.039 ± 0.013	0.484 ± 0.187	1.002 ± 0.002	1.5 ± 0.3	3.64
108	2017-03-01	CIR 2017-02-27	2017-03-02	0.045 ± 0.005	0.088 ± 0.035	1.008 ± 0.006	3.8 ± 0.6	33.5

Table 3
(Continued)

No.	FD start	Solar Activity	Minimum Flux Day	a	α	C	FD Amplitude (%)	MAR (GV)
109	2017-03-24	CIR 2017-03-20	2017-03-24	0.077 ± 0.008	0.301 ± 0.057	0.993 ± 0.003	4.2 ± 0.3	13
110	2017-03-28	CIR 2017-03-26	2017-04-02	0.068 ± 0.010	0.424 ± 0.078	0.997 ± 0.002	2.9 ± 0.3	5.9
111	2017-04-19	CIR 2017-04-18	2017-04-23	0.134 ± 0.005	0.184 ± 0.018	0.988 ± 0.003	9.3 ± 0.4	22.8
112	2017-05-16	CIR 2017-05-14	2017-05-16	0.064 ± 0.013	0.508 ± 0.115	0.994 ± 0.002	2.3 ± 0.3	3.29
113	2017-05-28	ICME 2017-05-27	2017-05-28	0.060 ± 0.006	0.075 ± 0.021	1.003 ± 0.007	5.1 ± 0.7	22.8
114	2017-06-17	CIR 2017-06-16	2017-06-17	0.029 ± 0.011	0.399 ± 0.213	0.990 ± 0.002	1.3 ± 0.3	5.9
115	2017-06-25	CIR 2017-06-23	2017-06-27	0.061 ± 0.005	0.203 ± 0.041	0.986 ± 0.003	4.1 ± 0.3	13
116	2017-07-16	ICME 2017-07-16	2017-07-17	0.216 ± 0.005	0.210 ± 0.011	0.986 ± 0.003	14.2 ± 0.3	16.6
117	2017-07-24	CIR 2017-07-20	2017-07-27	0.059 ± 0.004	0.138 ± 0.024	0.996 ± 0.003	4.4 ± 0.4	9.26
118	2017-08-01	CIR 2017-08-01	2017-08-02	0.167 ± 0.011	0.412 ± 0.039	0.998 ± 0.002	7.3 ± 0.3	8.48
119	2017-08-19	CIR 2017-08-16	2017-08-20	0.122 ± 0.007	0.316 ± 0.030	0.990 ± 0.002	6.5 ± 0.3	8.48
120	2017-09-07	ICME 2017-09-06	2017-09-07	0.026 ± 0.012	0.045 ± 0.051	1.004 ± 0.014	2.3 ± 1.3	48.5
121	2017-09-08	ICME 2017-09-07	2017-09-08	0.262 ± 0.004	0.196 ± 0.009	0.969 ± 0.003	17.7 ± 0.3	22.8
122	2017-10-24	CIR 2017-10-24	2017-10-25	0.120 ± 0.030	0.764 ± 0.167	0.997 ± 0.002	2.6 ± 0.3	5.9
123	2018-03-10*	ICME 2018-03-09						
124	2018-03-17	CIR 2018-03-14	2018-03-17	0.033 ± 0.005	0.224 ± 0.065	0.999 ± 0.003	2.1 ± 0.3	6.47
125	2018-03-23	CIR 2018-03-22	2018-03-24	0.060 ± 0.005	0.096 ± 0.021	0.994 ± 0.005	4.9 ± 0.5	11
126	2018-04-18*	CIR 2018-04-19						
127	2018-05-06	CIR 2018-05-05	2018-05-08	0.037 ± 0.005	0.160 ± 0.053	1.003 ± 0.004	2.7 ± 0.4	22.8
128	2018-05-17	CIR 2018-05-16	2018-05-18	0.053 ± 0.005	0.188 ± 0.041	1.000 ± 0.003	3.6 ± 0.3	9.26
129	2018-06-18	CIR 2018-06-17	2018-06-20	0.087 ± 0.009	0.373 ± 0.059	0.992 ± 0.002	4.1 ± 0.3	9.26
130	2018-06-23	CIR 2018-06-23	2018-06-23	0.044 ± 0.004	0.168 ± 0.041	1.001 ± 0.003	3.1 ± 0.4	11
131	2018-09-11	...						
132	2018-09-23	ICME 2018-09-23	2018-09-23	0.033 ± 0.006	0.228 ± 0.102	0.997 ± 0.003	2.1 ± 0.4	13
133	2018-11-10	CIR 2018-11-09	2018-11-13	0.043 ± 0.005	0.249 ± 0.060	0.991 ± 0.002	2.6 ± 0.3	10.1
134	2018-12-03	CIR 2018-12-01	2018-12-05	0.035 ± 0.004	0.095 ± 0.029	1.002 ± 0.004	2.9 ± 0.4	8.48
135	2018-12-25	...						
136	2019-01-05*	CIR 2019-01-04						
137	2019-01-24	CIR 2019-01-22	2019-01-27	0.026 ± 0.008	0.050 ± 0.038	1.005 ± 0.010	2.4 ± 0.9	33.5
138	2019-05-09	...						
139	2019-05-11	ICME 2019-05-10	2019-05-12	0.043 ± 0.005	0.158 ± 0.048	0.996 ± 0.004	3.2 ± 0.4	11
140	2019-07-09	CIR 2019-07-08	2019-07-10	0.047 ± 0.005	0.094 ± 0.030	1.003 ± 0.006	3.9 ± 0.6	33.5
141	2019-09-14	CIR 2019-09-12	2019-09-16	0.072 ± 0.011	0.478 ± 0.092	0.998 ± 0.002	2.8 ± 0.3	4.88
142	2019-10-25	CIR 2019-10-23	2019-10-29	0.057 ± 0.006	0.197 ± 0.043	1.003 ± 0.003	3.8 ± 0.4	5.37

FD can be associated with multiple solar activities and that these solar activities can occur on the same day.

ORCID iDs

Siqi Wang https://orcid.org/0000-0003-2056-4914
Veronica Bindi https://orcid.org/0000-0002-6706-0556
Cristina Consolandi https://orcid.org/0000-0003-4257-4187
Claudio Corti https://orcid.org/0000-0001-9127-7133
Christopher Light https://orcid.org/0000-0002-8403-2004
Nikolay Nikonov https://orcid.org/0000-0001-8088-187X
Andrew Kuhlman https://orcid.org/0000-0001-9156-6226

References

Aguilar, M., Cavasonza, L. A., Ambrosi, G., et al. 2021, PhRvL, 127, 271102
Ahluwalia, H., & Fikani, M. 2007, JGRA, 112, A08105
Alania, M., & Wawrzynczak, A. 2008, ASTRA, 4, 59
Alania, M. V., & Wawrzynczak, A. 2012, AdSpR, 50, 725
Alemanno, F., An, Q., Azzarello, P., et al. 2021, ApJL, 920, L43
Belov, A., Papaioannou, A., Abunina, M., et al. 2021, ApJ, 908, 5
Cane, H. V. 2000, in Cosmic Rays and Earth. Series: Space Sciences Series of ISSI, Vol. 10, ed. J. W. Bieber et al. (Dordrecht: Springer), 55
Clem, J., Guzik, T., Lijowski, M., et al. 1993, GeoRL, 20, 1743
Forbush, S. E. 1937, PhRv, 51, 1108
Grandin, M., Aikio, A. T., & Kozlovsky, A. 2019, JGRA, 124, 3871
Janvier, M., Démoulin, P., Guo, J., et al. 2021, ApJ, 922, 216
Kallaya, O., & Yeeram, T. 2021, Ap&SS, 366, 61
Klyueva, A., Belov, A., & Eroshenko, E. 2017, Ge&Ae, 57, 177
Light, C., Bindi, V., Consolandi, C., et al. 2020, ApJ, 896, 133
Lockwood, J. A. 1971, SSRv, 12, 658
Munini, R., Boezio, M., Bruno, A., et al. 2018, ApJ, 853, 76
Nieves-Chinchilla, T., Vourlidas, A., Raymond, J., et al. 2018, SoPh, 293, 1
Papaioannou, A., Belov, A., Abunina, M., et al. 2020, ApJ, 890, 101
Raghav, A., Shaikh, Z., Misal, D., et al. 2020, PhRvD, 101, 062003
Richardson, I. G. 2018, LRSP, 15, 1
Richardson, I. G., & Cane, H. V. 2010, SoPh, 264, 189
Usoskin, I., Braun, I., Gladysheva, O., et al. 2008, JGRA, 113, A07102